Modeling, Detecting, and Tracking Freezing of Gait in Parkinson Disease Using Inertial Sensors

G. V. Prateek , *Student Member, IEEE*, Isaac Skog , *Senior Member, IEEE*, Marie E. McNeely, Ryan P. Duncan , Gammon M. Earhart, and Arye Nehorai , *Life Fellow, IEEE*

Abstract—In this paper, we develop new methods to automatically detect the onset and duration of freezing of gait (FOG) in people with Parkinson disease (PD) in real time, using inertial sensors. We first build a physical model that describes the trembling motion during the FOG events. Then, we design a generalized likelihood ratio test framework to develop a two-stage detector for determining the zero-velocity and trembling events during gait. Thereafter, to filter out falsely detected FOG events, we develop a point-process filter that combines the output of the detectors with information about the speed of the foot, provided by a foot-mounted inertial navigation system. We computed the probability of FOG by using the point-process filter to determine the onset and duration of the FOG event. Finally, we validate the performance of the proposed system design using real data obtained from people with PD who performed a set of gait tasks. We compare our FOG detection results with an existing method that only uses accelerometer data. The results indicate that our method yields 81.03% accuracy in detecting FOG events and a threefold decrease in the false-alarm rate relative to the existing method.

Index Terms—Parkinson disease, freezing of gait, inertial sensors, accelerometer, gyroscopes, point-process filter.

I. INTRODUCTION

PARKINSON disease (PD) is a neuro-degenerative disorder that affects 1–1.5 million people in the United States alone. The main cause of PD is a loss of dopaminergic, sub-cortical neurons, which leads to motor impairments [1]. Many individuals with PD experience difficulty walking, the emergence of which is considered as a red flag for onset of disability [2].

Approximately 50% of people with PD experience freezing of gait (FOG), a "brief, episodic absence or marked reduction of forward progression of the feet despite the intention to walk" [3]. FOG events, which are a known risk factors for falls, occur suddenly, generally last for a few seconds, and tend to increase in frequency and duration as the disease progresses.

The most commonly prescribed medication to improve symptoms in people with PD is levodopa. The effective period of the drug varies between two and six hours [4], and decreases as the disease progresses [5]. Recent studies have shown that cueing techniques that apply spatial or temporal external stimuli associated with the motor activity enhance gait and reduce FOG [6], [7]. For example, auditory stimulation (see e.g., [8], [9]) and visual markers are used as cueing mechanisms to improve locomotor function in people with PD. Currently, to validate the severity of FOG, clinicians use patient questionnaires such as the new FOG-Questionnaire (NFOG-Q) [10] that rely on patient self-report. There is a growing need to develop automated methods for detecting FOG, with the ultimate goal of being able not only to measure but also to predict and prevent episodes of FOG.

In the last decade, methods using wearable technology for monitoring and assessing gait patterns and FOG have been developed with varying success. These methods variously employ a) electromyography (EMG) sensors [11], [12]; b) force resistive sensors [13], [14]; c) video-based gait analysis [15], [16]; or d) inertial sensors (accelerometers and gyroscopes) [4], [17]–[24]. In the case of inertial sensors, the spectral characteristics of the accelerometer signal in the vertical direction provide information that is helpful in distinguishing FOG patterns from normal PD gait patterns. For example, researchers use the spectral characteristics of the accelerometer signal to develop a four stage automatic gait detection algorithm [17], [18]. In prior reports, a freeze-index (FI) is defined as the ratio of the square of the power spectrum in two different non-overlapping frequency bands [19]. An extension of the FI method for a variable size window and online detection is presented in [20], [21], [25]. The use of machine learning methods to classify features extracted from the accelerometer signal that capture the uncoordinated nature of the gait, such as trembling of the feet, short stride lengths, and unstable walking, is explored in [22]–[24]. However, the preceding methods do not necessarily present a signal model that captures the FOG patterns explicitly, and they use long window lengths to compute the spectral characteristics of the accelerometer signal, which leads to delays when
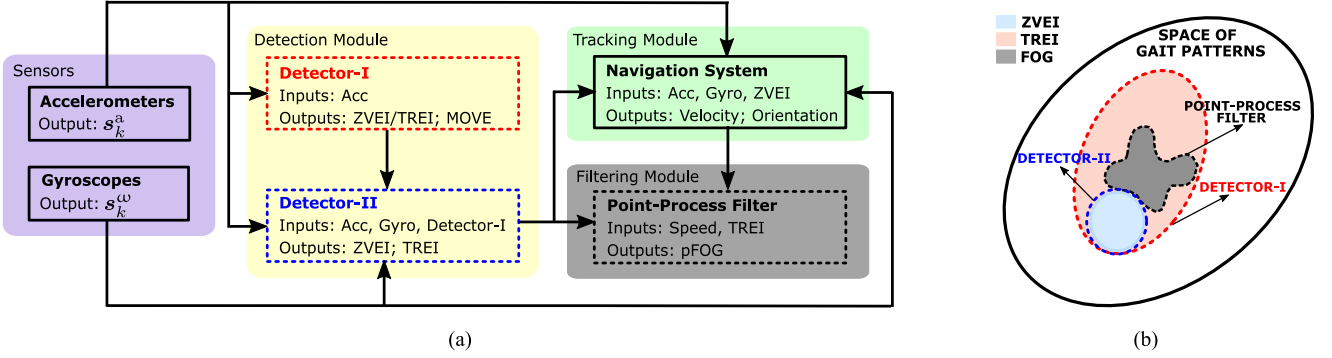
Fig. 1. Using the accelerometer data, Detector-I (red-dashed rectangle in (a)) filters out gait patterns (MOVE) that are neither ZVEI nor TREI (red-dashed ellipse in (b)). Detector-II (blue-dashed rectangle in (a)) uses information from the gyroscope, to distinguish ZVEI (blue-dashed circle in (b)) from TREI. The region detected by Detector-I also contains gait patterns with energy information similar to that of TREI (orange region in (b)). To identify FOG (gray region in (b)), a point-process filter (black-dashed rectangle in (a)) combines the information of Detector-II with the speed of the foot, provided by the inertial navigation system. Regions with high probability of freezing of gait indicate FOG (black-dashed outline in (b)). FOG is a reflection of both ZVEI and TREI, and thus the FOG region which lies inside TREI region shares a common boundary with the ZVEI. (a) A block diagram of the system used to calculate the pFOG. (b) An illustration of the subsets of the gait patterns that the different detectors and point-process filter identify.

determining the onset of the FOG event. Further, methods developed using machine learning techniques lack explanatory power and provide limited utility for understanding the structure of the data [26].

To overcome these drawbacks, here we develop a physical model for the sensor data, design statistical signal processing methods to detect FOG based on its patterns, and compute the probability of FOG (pFOG). The goal of this work is to automatically detect the onset and duration of FOG in people with PD in real-time. The modeling results of this work can also help understand the physical mechanism of gait patterns in PD.

Notations: The following general notation will be used throughout the paper. Bold uppercase and lowercase letters denote a matrix and vector, respectively. Superscript/subscript a and ω represent accelerometer and gyroscope signals, respectively. For any real matrix $\boldsymbol{A}$, $\boldsymbol{A}^T$, $\boldsymbol{A}^{-1}$, and $\text{Tr}\{\boldsymbol{A}\}$, denote the transpose, inverse, and trace of $\boldsymbol{A}$, respectively. $\boldsymbol{I}_n$ represents an identity matrix of n-dimension. $\mathbb{1}_n$ is an n-dimensional column vector of all ones. We denote ℓ_2-norm as $\|\cdot\|$. The expectation and covariance operator are denoted as $\mathbb{E}\{\cdot\}$ and $\text{Cov}\{\cdot\}$, respectively. The random scalar $x \sim \chi_n^2$ has a chi-square distribution with n degrees of freedom. The random n-dimensional vector $\boldsymbol{x} \sim \mathcal{N}(\boldsymbol{p}, \boldsymbol{\Sigma})$ is multivariate Gaussian, distributed with mean $\boldsymbol{p}$ and covariance $\boldsymbol{\Sigma}$.

II. SYSTEM OVERVIEW

To detect and track FOG in real-time, we propose the system design as shown in Fig. 1. To capture gait motion, we use a MEMS-based inertial measurement unit (IMU) which consists of a three-axis accelerometer and a three-axis gyroscope. The IMU is strapped to the heel region of the foot of the participant, as shown in Fig. 2. Our system design consists of three modules, namely the detection, tracking, and filtering modules.

The detection module includes a two-step detection algorithm to determine instances of zero-velocity event intervals (ZVEI) and trembling event intervals (TREI). In Section III-B, we
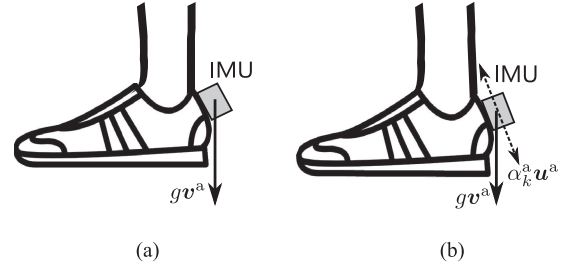

Fig. 2. Gait patterns. (a) Zero-velocity event intervals (ZVEI) are associated with the flat foot phase of a gait cycle. (b) Trembling event intervals (TREI) are associated with the heel lift-off and heel strike phase of a gait cycle.

derive the first detector which can detect ZVEI or TREI; this detector cannot separate these two events. In other words, the goal of the first detector is to filter out gait patterns that cannot be classified as ZVEI or TREI. In Section III-C, we derive the second detector, which uses information from the gyroscope to distinguish ZVEI from TREI. This is necessary because the ZVEI/TREI identified by the first detector contains some gait patterns modeled as trembling events, but not associated with FOG. The second detector only detects ZVEI and cannot filter out those gait patterns identified as TREI which are not associated with FOG. Therefore, to detect the FOG region, which is a reflection of both ZVEI and TREI, we use the fact that FOG is characterized by small foot speeds [27], [28]. Note that in Fig. 1(b), the FOG region lies inside TREI region and shares a common boundary with the ZVEI region.

In Section IV, we briefly describe the functionality of the foot-mounted inertial navigation system (INS), which computes the position, velocity, and orientation estimates of the sensor during gait. We use an INS in the tracking module to estimate the speed (ℓ_2-norm of the velocity vector) of the foot. To improve the detection of the FOG episodes, we develop a point-process filtering module in Section V. The point-process filter computes the pFOG by combining the output of the detectors with the

information about the speed of the foot. The time periods with high pFOG determine the onset and duration of the FOG event. To validate the system design, we use the experimental setup described in Section VI. With the help of an illustrative example, in Section VII, we demonstrate the output of each system module. In Section VIII, we present the experimental results. Our conclusions and directions for possible future work are presented in Section IX.

III. DETECTION MODULES

In this section, we develop a physical model to describe the signal from the inertial sensor during the zero-velocity and trembling event, and design a statistically-based approach to detect these gait patterns. In particular, we develop a two-step detection algorithm to identify zero-velocity and trembling events. We formulate the two-step detection algorithm as a hypothesis testing problem and solve it using the generalized likelihood ratio test (GLRT) framework [29].

A. Signal Model and Statistics

If $\boldsymbol{y}_k^a \in \mathbb{R}^{3\times1}$ and $\boldsymbol{y}_k^\omega \in \mathbb{R}^{3\times1}$ denote the measurements of a three-axis accelerometer and a three-axis gyroscope, respectively, at time instant k, then these measurements can be modeled as

$$\boldsymbol{y}_k^a = \boldsymbol{s}_k^a + \boldsymbol{e}_k^a$$
$$\boldsymbol{y}_k^\omega = \boldsymbol{s}_k^\omega + \boldsymbol{e}_k^\omega. \quad (1)$$

Here, $\boldsymbol{s}_k^a$ and $\boldsymbol{s}_k^\omega$ denote the true specific force and angular velocity experienced by the accelerometer and gyroscope, respectively. Further, $\boldsymbol{e}_k^a$ and $\boldsymbol{e}_k^\omega$ denote the measurement errors of the accelerometer and gyroscope, which are assumed to be white, mutually uncorrelated, and Gaussian distributed with zero mean and covariance matrices $\sigma_a^2 \boldsymbol{I}_3$ and $\sigma_\omega^2 \boldsymbol{I}_3$, respectively.

Based on clinical observations, FOG patterns include alternating trembling in the lower extremities (includes the hip, knee, and ankle joints, and the bones of the thigh, leg, and foot), and no movement of the limbs and trunk [30], [31]. Short, shuffling steps, not specific to or necessarily related to freezing, are observed in parkinsonian gait [32], [33]. Festination is usually associated with a progressive shortening and quickening of steps that often results in a freeze where forward/backward progression ceases [34].

We model gait patterns such as no movement of limbs in FOG, and short, shuffling steps in parkinsonian gait, as ZVEI. These events are associated with the flat foot phase of a gait cycle. ZVEI are defined as the time instances when the IMU is stationary, i.e., the IMU has a constant position and orientation; see Fig. 2(a) for illustration. During ZVEI, the accelerometer measures only the earth's gravitational acceleration, i.e., $g\boldsymbol{v}^a$, where g and $\boldsymbol{v}^a$ are the magnitude and direction of a unit vector along the gravity. For parkinsonian gait with short, shuffling steps, the duration of the ZVEI are smaller than regular steps during normal PD gait. Further, we model gait patterns such as alternating trembling in FOG, and short, quickening steps on the toes and forepart of the feet in festinating gait, as TREI. These events are associated with heel lift-off and heel strike phase of a gait cycle. TREI are modeled as the motion of the IMU about an unknown fixed axis, and of unknown magnitude which depends on the severity of the trembling; see Fig. 2(b) for illustration. During trembling event, the accelerometer measures the sum of the inertial acceleration and gravitational acceleration, i.e., $\alpha_k^a \boldsymbol{u}^a + g\boldsymbol{v}^a$, where α_k^a and $\boldsymbol{u}^a$ are the magnitude and direction of a unit vector along the trembling axis. In this case, the accelerometer cannot distinguish between the axis aligned with the gravity field and trembling.

B. Detector-I

The goal of the first detector is to detect zero-velocity and trembling events, and filter out gait patterns that are not associated with FOG. The detection problem can be formulated as

$$\mathcal{H}_1, \mathcal{H}_2 \triangleq \text{IMU is stationary } or \text{ experiencing trembling}$$
$$\mathcal{H}_0 \triangleq \text{Otherwise.} \quad (2)$$

For notation, we denote $\mathcal{H}_1$ and $\mathcal{H}_2$ together as $\mathcal{H}_{1,2}$. Under $\mathcal{H}_{1,2}$, the specific force measured by the accelerometers in (2), in the time window Ω_N of size N consisting of the time samples $\{k, \ldots, k+N-1\}$, can be modeled as

$$\mathcal{H}_1, \mathcal{H}_2 : \forall k \in \Omega_N : \boldsymbol{s}_k^a = \alpha_k^a \boldsymbol{u}^a + g\boldsymbol{v}^a,$$
$$\mathcal{H}_0 : \exists k \in \Omega_N : \boldsymbol{s}_k^a \neq \alpha_k^a \boldsymbol{u}^a + g\boldsymbol{v}^a. \quad (3)$$

Given the signal model in (3), it can be shown (see Appendix B of the supplementary material) that the generalized loglikelihood ratio test for detecting ZVEI and TREI are given by

$$T_{\mathrm{D}_1}(\boldsymbol{y}^a) = \frac{1}{N} \sum_{k \in \Omega_N} \left\{ \frac{1}{\sigma_a^2} \|\boldsymbol{y}_k^a - g\hat{\boldsymbol{v}}^a\|_{\boldsymbol{P}_{\hat{\boldsymbol{u}}^a}^\perp}^2 \right\} \mathop{\lessgtr}\limits_{<}^{\mathcal{H}_{12}} \gamma'_{\mathrm{D}_1}, \quad (4)$$

where $\hat{\boldsymbol{v}}^a$ and $\hat{\boldsymbol{u}}^a$ denote the estimated unit vectors in the direction of earth's gravitational acceleration vector and the trembling axis, respectively. Here, $\boldsymbol{y}^a = [(\boldsymbol{y}_k^a)^T, \ldots, (\boldsymbol{y}_{k+N-1}^a)^T]^T$, $\boldsymbol{P}_{\hat{\boldsymbol{u}}^a}^\perp = \boldsymbol{I} - \hat{\boldsymbol{u}}^a(\hat{\boldsymbol{u}}^a)^T$, and γ'_{D_1} is the detector threshold.

To understand the intuitive meaning of (4), let us assume that the measurement error in the accelerometer is zero. When the IMU is stationary, the output from the accelerometer is given as $g\boldsymbol{v}^a$. If the estimate of $\hat{\boldsymbol{v}}^a$ is close to $\boldsymbol{v}^a$, then the weighted norm in (4) is close to zero. When the IMU experiences trembling about a fixed axis, $\boldsymbol{u}^a$, then the output of the accelerometer consists of both a gravitational and a trembling component. In Appendix A of the supplementary material, we show that $\hat{\boldsymbol{u}}^a$ is the eigenvector in the direction of maximum eigenvalue of $\boldsymbol{G}^a = \sum_{k \in \Omega_N} (\boldsymbol{y}_k^a - g\hat{\boldsymbol{v}}^a)(\boldsymbol{y}_k^a - g\hat{\boldsymbol{v}}^a)^T$. If the estimate of $\hat{\boldsymbol{v}}^a$ closely matches the true direction of the gravitational vector, $\boldsymbol{v}^a$, then, the matrix $\boldsymbol{G}^a$ captures the outer product of the accelerometer output along the trembling axis. The matrix $\boldsymbol{G}^a$ is symmetric and positive semi-definite. For any symmetric and positive semi-definite matrix, the eigenvector corresponding to the maximum eigenvalue represents the direction of the semi-major axis, and its eigenvalue represents the length of the semi-major axis. Therefore, the eigenvector, $\hat{\boldsymbol{u}}^a$, represents

the estimated trembling axis. If the estimated trembling axis, $\hat{\boldsymbol{u}}^a$, matches the direction of the true trembling axis, $\boldsymbol{u}^a$, then the weighted norm in (4) is zero, because the projection of $\hat{\boldsymbol{u}}^a$ on $\boldsymbol{P}_{\hat{\boldsymbol{u}}^a}^{\perp}$ is zero.

C. Detector-II

To distinguish ZVEI from TREI, we develop a second detector. Based on the hypotheses $\mathcal{H}_1$ and $\mathcal{H}_2$ defined in the previous subsection, we get

$$\mathcal{H}_1 \triangleq \text{ IMU is stationary (ZVEI)}$$

$$\mathcal{H}_2 \triangleq \text{ IMU is experiencing trembling (TREI).} \quad (5)$$

Under $\mathcal{H}_1$, the IMU has a constant position and orientation. Because the gyroscopes are highly sensitive to angular motion, we include angular velocity measurements in the hypothesis testing problem in (5). Mathematically, under the assumption that the hypothesis $\mathcal{H}_{1,2}$ is true, the signal model for the two hypothesis in (5) can be written as

$$\mathcal{H}_1 : \begin{cases} \forall k \in \Omega_N : \boldsymbol{s}_k^a = g\boldsymbol{v}^a \iff \alpha_k^a = 0 \\ \forall k \in \Omega_N : \boldsymbol{s}_k^\omega = \boldsymbol{0} \end{cases}$$

$$\mathcal{H}_2 : \begin{cases} \exists k \in \Omega_N : \boldsymbol{s}_k^a = \alpha_k^a \boldsymbol{u}^a + g\boldsymbol{v}^a, \iff \alpha_k^a \neq 0 \\ \exists k \in \Omega_N : \boldsymbol{s}_k^\omega \neq \boldsymbol{0}. \end{cases} \quad (6)$$

Given the signal model in (6), it can be shown (see Appendix B of the supplementary material) that the generalized loglikelihood ratio test for detecting ZVEI or TREI are given by

$$T_{\mathrm{D}_2}(\boldsymbol{y}) = \frac{1}{N} \sum_{k \in \Omega_N} \left\{ \frac{1}{\sigma_\omega^2} \|\boldsymbol{y}_k^\omega\|^2 \right.$$

$$\left. + \frac{1}{\sigma_a^2} \left[\left\| \boldsymbol{y}_k^a - g\frac{\bar{\boldsymbol{y}}^a}{\|\bar{\boldsymbol{y}}^a\|} \right\|^2 - \|\boldsymbol{y}_k^a - g\hat{\boldsymbol{v}}^a\|_{\boldsymbol{P}_{\hat{\boldsymbol{u}}^a}^{\perp}}^2 \right] \right\} \overset{\mathcal{H}_1}{\underset{}{\lessgtr}} \gamma'_{\mathrm{D}_2}, \quad (7)$$

where $\boldsymbol{y}$ is the concatenation of the accelerometer and gyroscope measurements given by $[(\boldsymbol{y}^a)^T, (\boldsymbol{y}^\omega)^T]^T$, $\boldsymbol{y}^\omega = [(\boldsymbol{y}_k^\omega)^T, \dots, (\boldsymbol{y}_{k+N-1}^\omega)^T]^T$, $\bar{\boldsymbol{y}}^a = (1/N) \sum_{k \in \Omega_N} \boldsymbol{y}_k^a$, and γ'_{D_2} is the detector threshold.

To understand the intuitive meaning of (7), let us again assume that the measurement error is zero for both the accelerometer and gyroscope. When the IMU is stationary, i.e., during zero-velocity event, the first term contains only error measurements, which are set to zero. The last term in (7) follows the same explanation as before, i.e., when the estimates of $\hat{\boldsymbol{v}}^a$ and $\hat{\boldsymbol{u}}^a$ match the true direction of the gravity vector and trembling axis, respectively, then the last term in (7) goes to zero. Further, when the IMU is stationary, the average mean vector of the measured accelerometer data seen in the window Ω_N, denoted as $\bar{\boldsymbol{y}}^a$, is the same as the measured accelerometer data, which is given as $g\boldsymbol{v}^a$. Due to this, the second term in (7) also goes to zero. Therefore, under the assumption that the IMU is stationary and the measurement error is zero, the test statistic in (7) is close to zero. However, during a trembling event in Fig. 2 and under the assumptions that the measured errors are zero, the last term in (7) goes to zero when the estimates $\hat{\boldsymbol{u}}^a$ and $\hat{\boldsymbol{v}}^a$ are close to

the true values. The first and second terms are non-zero because gyroscope measurements are non-zero and accelerometer measurements contain both gravitational and specific force components. Therefore, the test statistic in (7) is non-zero under $\mathcal{H}_2$.

Observation: The signal model in (3) captures a large set of gait patterns that are not associated with FOG. The signal model in (6) distinguishes zero-velocity events from trembling events, but cannot filter out gait patterns that are not associated with FOG. In other words, the trembling events identified by the Detector-II also include falsely detected FOG events. Therefore, to filter out these falsely detected events, we use the fact that FOG events are associated with small foot speeds [27], [28]. This is done using a point-process filter, which fuses the output from the detector framework with the speed information provided by a foot-mounted inertial navigation system.

IV. TRACKING MODULE

In this section, we present a brief overview of the tracking module used in the system design as shown in Fig. 1. Foot-mounted inertial navigation systems (INSs) are frequently used for ambulatory gait analysis [35]–[39] and pedestrian navigation [40]–[42]. We use a zero-velocity aided foot-mounted inertial navigation system described in [43]–[45] to estimate the speed of the foot during the gait. The INS uses the accelerometer and gyroscope sensor measurements along with the ZVEI [46] to estimate the position, velocity, and orientation of the foot via dead reckoning [47].

V. FILTERING MODULE

In this section, we describe the filtering module in the system design in Fig. 1. We develop a point-process which is characterized by the conditional intensity function [48], whose parameters are modeled as a Gaussian autoregressive model [49]–[52]. By combining the information about the speed of the foot with the detected TREI via a conditional intensity function, we compute the probability of FOG (pFOG).

Recall that Detector-I identifies the zero-velocity and trembling events, and Detector-II only separates zero-velocity events from trembling events. The edges of the TREI also contain information of either the beginning or ending of ZVEI, which represents FOG patterns, characterized by small foot speeds. Therefore, we detect the edges of the TREI and model them as spikes generated from a point-process. The spikes are divided into equal segments or bins of length $B = \Delta F_s$ samples, where Δ is the width of the bin interval in seconds and F_s is the sampling rate of the IMU. Let δB_k and b_k denote an indicator variable[1] and the number of spikes in the interval $((k-1)\Delta, k\Delta], k \in \mathbb{N}$, respectively. Further, let w_k denote a weight associated with each bin interval. FOG patterns such as trembling and short shuffling steps are characterized by small foot speeds [27]. To identify bins with small foot speeds, we first compute the average bin speed for the bin intervals $((k-1)\Delta, k\Delta]$. Then, we use a Gaussian kernel with zero mean and σ_s standard deviation to assign larger weights to bins with smaller average foot speeds.

---

[1]$\delta B_k = 1$, if $b_k \neq 0$ and $\delta B_k = 0$, if $b_k = 0$.

In our proposed method, the system parameter σ_s is considered as a participant-specific tunable parameter. As σ_s decreases, the bin weights corresponding to smaller foot speeds increase.

Let $\delta \boldsymbol{B}_{1:k} = [\delta B_1, \ldots, \delta B_k]$, $\boldsymbol{b}_{1:k} = [b_1, \ldots, b_k]$, and $\boldsymbol{w}_{1:k} = [w_1, \ldots, w_k]$ denote the activity of observable parameters up to time $k\Delta$. Let $\boldsymbol{H}_k = [\delta \boldsymbol{B}_{k-l-1:k-1}, \boldsymbol{b}_{k-l-1:k-1}, \boldsymbol{w}_{k-l-1:k-1}]$ denote the history of the activity of the spikes observed in the interval $((k-l-1)\Delta, (k-1)\Delta]$, where l represents length of the history. Let $\boldsymbol{\theta}_k = [\theta_{k,0}, \ldots, \theta_{k,l-1}]^T \in \mathbb{R}^l$ denote a latent parameter vector. We model the number of spikes observed in the k-th interval as a binomial distribution with probability mass function given by

$$f(b_k|\boldsymbol{\theta}_k, \boldsymbol{H}_k) = \binom{B}{b_k} p_k^{b_k} (1-p_k)^{(B-b_k)}, \qquad (8)$$

where

$$p_k = \frac{\exp(\lambda_k(\boldsymbol{\theta}_k))}{1 + \exp(\lambda_k(\boldsymbol{\theta}_k))} \quad \text{and} \qquad (9)$$

$$\lambda_k(\boldsymbol{\theta}_k) = \alpha + \beta \left(\sum_{i=0}^{l-1} \theta_{k,i}^2 w_{k-i} \delta B_{k-i} \right). \qquad (10)$$

In (9), p_k is a sigmoid function that represents instantaneous pFOG in the interval $((k-1)\Delta, k\Delta]$, α denotes a fixed background firing rate, and β is a fixed scaling parameter. The exponential term is defined as the conditional intensity function [48] and the log-exponential is denoted as $\lambda_k(\boldsymbol{\theta}_k)$. In (10), we model the history of spikes as an auto-regressive process where $\theta_{k,i}$ represents the auto-regressive coefficients. The parameters that define the conditional intensity function in (10) are either fixed or observable, except for $\boldsymbol{\theta}_k$ (a latent parameter vector), which is modeled as a linear evolution process with Gaussian errors [49]–[53]. We define the evolution process of the latent parameter as

$$\boldsymbol{\theta}_{k+1} = \boldsymbol{F}_k \boldsymbol{\theta}_k + \boldsymbol{\eta}_k, \qquad (11)$$

where $\boldsymbol{F}_k$ is the system evolution matrix and $\boldsymbol{\eta}_k$ is zero-mean additive Gaussian noise with covariance $\boldsymbol{Q}_k$. The probability of freezing of gait (pFOG) is given as

$$p_k' = \frac{1}{l} \sum_{i=0}^{l-1} p_{k-i}.$$

Applying Bayes' rule to (8) and (11), the posterior density of the parameter vector in the k-th interval is given as

$$f(\boldsymbol{\theta}_k|b_k, \boldsymbol{H}_k) = \frac{f(b_k|\boldsymbol{\theta}_k, \boldsymbol{H}_k) f(\boldsymbol{\theta}_k|\boldsymbol{H}_k)}{f(b_k|\boldsymbol{H}_k)}, \qquad (12)$$

where

$$f(\boldsymbol{\theta}_k|\boldsymbol{H}_k) = \int f(\boldsymbol{\theta}_k|\boldsymbol{\theta}_{k-1}, \boldsymbol{H}_k) f(\boldsymbol{\theta}_{k-1}|b_{k-1}, \boldsymbol{H}_{k-1}) d\boldsymbol{\theta}_{k-1}$$

$$= \int f(\boldsymbol{\theta}_k|\boldsymbol{\theta}_{k-1}) f(\boldsymbol{\theta}_{k-1}|b_{k-1}, \boldsymbol{H}_{k-1}) d\boldsymbol{\theta}_{k-1}. \quad (13)$$

The last equality comes from (11), where $\boldsymbol{\theta}_k$ does not depend on the aggregate history of the spikes, $\boldsymbol{H}_k$. Based on (11), we assume that the latent parameter vector, $\boldsymbol{\theta}_k$, follows a Gaussian distribution. There is no closed form expression for the Bayesian recursive filter in (12) and (13). Therefore, we develop the approximate filters based on the Gaussian approximations. The Gaussian approximation of the posterior density of the latent parameter vector in (11) can be motivated by the fact that the Binomial distribution in (8) converges towards a Gaussian distribution as the number of samples in each bin, B, increase. Let $\boldsymbol{\theta}_{k|k-1} = \mathbb{E}[\boldsymbol{\theta}_k|\boldsymbol{H}_k]$ and $\boldsymbol{P}_{k|k-1} = \text{Cov}[\boldsymbol{\theta}_k|\boldsymbol{H}_k]$ denote the mean and the covariance of one-step prediction density. Similarly, let $\boldsymbol{\theta}_{k|k} = \mathbb{E}[\boldsymbol{\theta}_k|b_k, \boldsymbol{H}_k]$ and $\boldsymbol{P}_{k|k} = \text{Cov}[\boldsymbol{\theta}_k|b_k, \boldsymbol{H}_k]$ denote the mean and the covariance of the posterior distribution. Then, using the Laplace Gaussian filter approximation method [52], [53], the point-process filter equations are given as

$$\boldsymbol{\theta}_{k|k-1} = \boldsymbol{F}_k \boldsymbol{\theta}_{k-1|k-1}, \qquad (14a)$$

$$\boldsymbol{P}_{k|k-1} = \boldsymbol{F}_k \boldsymbol{P}_{k-1|k-1} \boldsymbol{F}_k^T + \boldsymbol{Q}_k, \qquad (14b)$$

$$\boldsymbol{\theta}_{k|k} = \boldsymbol{\theta}_{k|k-1} + \boldsymbol{P}_{k|k} \left[(b_k - Bp_k) \frac{\partial \lambda_k(\boldsymbol{\theta}_k)}{\partial \boldsymbol{\theta}_k} \right]_{\boldsymbol{\theta}_{k|k-1}}, \qquad (14c)$$

$$(\boldsymbol{P}_{k|k})^{-1} = (\boldsymbol{P}_{k|k-1})^{-1} + \left[(Bp_k - b_k) \frac{\partial^2 \lambda_k(\boldsymbol{\theta}_k)}{\partial \boldsymbol{\theta}_k \partial \boldsymbol{\theta}_k^T} \right.$$
$$\left. + Bp_k(1-p_k) \frac{\partial \lambda_k(\boldsymbol{\theta}_k)}{\partial \boldsymbol{\theta}_k} \frac{\partial \lambda_k(\boldsymbol{\theta}_k)}{\partial \boldsymbol{\theta}_k}^T \right]_{\boldsymbol{\theta}_{k|k-1}}. \qquad (14d)$$

We provide the details of the derivation of (14a)–(14d) in Appendix C of the supplementary material. Equations (14a) and (14b) are the mean and covariance of a one-step prediction distribution. Similarly, (14c) and (14d) are the mean and co-variance of the posterior distribution, respectively. The second term in (14c) is the learning rate, analogous to the posterior update step of a Kalman filter. The term $(b_k/B - p_k)$ in (14c) is the innovation term, because b_k/B represents the probability of spikes in the measurement model and p_k is the probability of spikes in the state model, observed in the k-th time interval. However, unlike the Kalman filter posterior update step, here the posterior update step depends on the posterior update co-variance matrix instead of the prediction covariance matrix. We compute p_k in (9), evaluated at $\boldsymbol{\theta}_k = \boldsymbol{\theta}_{k|k}$ at every time instance $k\Delta$, to obtain the instantaneous pFOG.

VI. EXPERIMENTAL SETUP AND DATA COLLECTION

In this section, we present the details of our experimental setup to assess gait in people with PD. We define the terminology of the scoring method required for tuning the parameters of the detector and the point-process filter. We also provide a brief description of the data collection mechanism and the hardware used in the experimental setup.

A. Experiments

To assess gait, we assigned five different tasks that are likely to trigger a FOG event. The list of the tasks and their descriptions are given in Table I. As a reference system, we use video-based

TABLE I
BALANCE ASSESSMENT TASKS AND THEIR DESCRIPTIONS

Task	Description of the task
BACK	The participant was asked to walk backwards at a comfortable pace along a 3 meter straight path. On reaching the end, the participant made a $180°$ turn and re-traversed the path in the next trial.
BLOCK	A wood block 6 inches high, 24 inches wide, and 14.5 inches deep was placed between two cones. The total distance between the center of each cone and the nearest edge of the block was 22.5 inches. The participant was asked to start between one of the cones and the block, step up onto the block and step down between the block and the second cone. The participant made a $180°$ turn in the small space between the block and the cone, and repeated the trial.
EIGHT	The participant was asked to follow a figure-eight trajectory around two cones placed 1.5 meters apart (cone center to cone center). Two chairs were placed with the backs inward, approximately shoulder width apart at the center of the figure-eight loop to create a narrow space. The participants started next to a cone at one end of the figure-eight loop, completed the figure-eight (traveling through the narrow space), and positioned themselves on the other side of the first cone for the next figure-eight.
NARROW	The participant was asked to walk along a path 3 meters long, with three sets of chairs placed with the backs inward, about shoulder width apart in the middle 1.5 meters of the path. At the end of the 3 meter path, the participant made a $180°$ turn and re-traversed the path in the next trial.
TURN	The participant was asked to do an in-place $180°$ turn. The participant began by standing stationary and was told to turn either right or left to face the wall behind them.

technology to determine the time instances of FOG. With the help of trained gait analysis experts, we mark the instances of FOG observed in the videos with a temporal resolution of one second. The experts watched each video together and came to consensus on the presence and timing of definite or potential freezing episodes. The synchronization of the video and IMU data is done manually.

B. Metrics

We define four metric variables that are used to evaluate the performance of the system design. The definition of each metric is as follows:

1) *Detection Length:* (DL) is defined as the length of the overlapping regions detected using both video data and the inertial sensor based method, for an episode of FOG. In other words, DL reflects the times when both methods agree that FOG is present.

2) *Missed Detection Length:* (MDL) is defined as the length of the non-overlapping regions between the FOG instances detected using video data and the inertial sensor based method, for an episode of FOG. When the inertial sensor based method fails to detect a FOG instance detected by the video data in either foot, then the length of that instance of FOG is also considered as MDL.

3) *False Alarm Length:* (FAL) is defined as the length of the non-overlapping region which is detected as a FOG instance by the inertial sensor based method, but not by the experts marking the video data.

4) *Total Length:* (TL) is defined as the total length of the IMU data (the same as the duration of the video data).

In Fig. 3, we present an illustration of DL, FAL, and MDL. Based on the metric variables, we define two performance metrics, namely, the true positive rate (TPR) or sensitivity, and the false alarm rate (FAR):

$$\text{TPR} = \frac{\text{DL}}{\text{DL} + \text{MDL}} \quad \text{and} \quad \text{FAR} = \frac{\text{FAL}}{\text{TL}}. \quad (15)$$
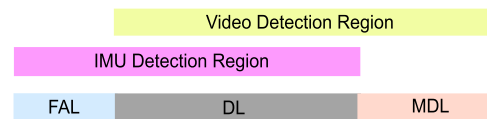

Fig. 3. An illustration of FAL, DL, and MDL. The overlapping region between the video and inertial sensor method is the detection length (gray color). The region detected by the video but not by the inertial sensor method is the missed detection length (light orange color). The region detected by the inertial sensor method but not by the video is the false alarm length (light blue color).

If TPR is close to one, then the episodes of FOG detected by the IMU match closely with the video data. Similarly, if FAR is close to zero, then the number of falsely detected FOG episodes is small. We say that an inertial sensor based algorithm performs as well as the video-based method if both TPR and $1 - \text{FAR}$ are close to one. When $\text{DL} = 0$ and $\text{MDL} = 0$, we say the $\text{TPR} = 1$, because no FOG episodes were detected by the video data nor by the algorithm using the IMU data.

C. Data Collection and Hardware

We use the Openshoe module to collect the accelerometer and gyroscope sensor data [43]. The sensors operate at a sampling frequency of $F_s = 1000$ Hz. We tape the sensor module to the heel of each shoe firmly, as shown in Fig. 2. The choice of the sensor location [4] enables us to compute gait parameters such as speed of the foot which can be useful in understanding the underlying mechanism of FOG. The sensors are powered by micro-USB cords whose other ends are plugged into a USB-port of a laptop. The laptop, which weighs less than 1.2 kilograms, is placed in a backpack carried by the participant. Cords are firmly strapped around each leg, so that they did not interfere with gait and there are minimal cord movements captured by the sensors.

VII. ILLUSTRATIVE EXAMPLE

In this section, with the help of an illustrative example, we demonstrate the output of each module of the proposed system design in Fig. 1. In particular, we use the inertial sensor data for
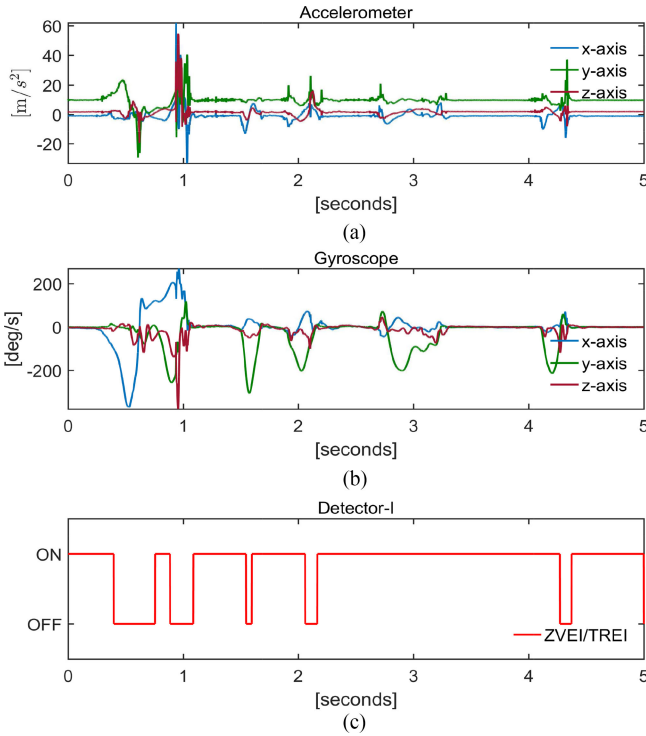
Fig. 4. ZVEI/TREI detected by Detector-I for TT004–BLOCK task. (a) Three-axis accelerometer signal. (b) Three-axis gyroscope signal. (c) Output of Detector-I (ZVEI/TREI).
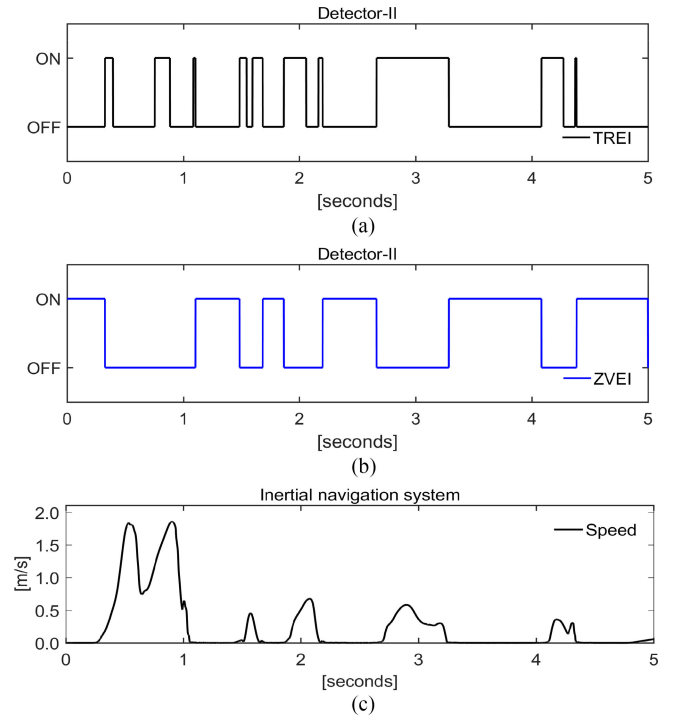

Fig. 5. Detector-II separates ZVEI from TREI. The inertial navigation system estimates the speed of the foot. (a) Output of Detector-II (TREI). (b) Output of Detector-II (ZVEI). (c) Output of the INS (speed of the foot).

participant identity (PID) TT004, performing the BLOCK task, during which the participant experiences a turning freeze.

A. Detector-I

The goal of Detector-I is to detect shuffling or trembling motion intervals, which are modeled as ZVEI and TREI, respectively. In Fig. 4(a) and (b), we plot the outputs of the three-axis accelerometer and the three-axis gyroscope sensor, respectively. In Appendix D of the supplementary material, we demonstrate the procedure to obtain the system parameters for Detector-I, using video data as the reference system. We set the size of the window $\Omega_N = 100$, the standard deviation of the accelerometer signal $\sigma_a = 1.0$, and the threshold of Detector-I $\gamma'_{D_1} = 34.53$. The output of Detector-I based on the test statistic in (4) is shown in Fig. 4(c). Detector-I in Fig. 4(c) is ON when the angular velocities measured by the gyroscope are zero and the specific force measured by the accelerometer in the y-axis is 9.8 m/s^2, indicating ZVEI. Further, Detector-I is also ON at some non-zero velocity instances, indicating possible TREI associated with FOG.

B. Detector-II and INS

As stated previously, the goal of Detector-II is to distinguish ZVEI from TREI based on the output of Detector-I. We refer to Appendix E of the supplementary material to obtain the design parameters of Detector-II. We use the same window length Ω_N as in Detector-I. In addition, we set the standard deviation of the gyroscope $\sigma_\omega = 0.8$ and the threshold $\gamma'_{D_2} = 2.00$. The output

of Detector-II, based on the test statistic in (7), is shown in Fig. 5(a) and (b). In Fig. 5(b), Detector-II detects ZVEI which can be verified with the information about the speed of the foot shown in Fig. 5(c). When zero-velocity updates are ON, the speed of the foot is close to zero. The time intervals that are not identified as ZVEI by Detector-II are considered as TREI, as shown in Fig. 5(a). However, not all the TREI are associated with FOG. Hence, to filter out falsely detected TREI that are not associated with FOG, we use the proposed point-process filter.

C. Point-Process Filter

Recall that the goal of the point-process filter is to filter out the falsely detected FOG events in the TREI. The edges in the TREI contain information about both ZVEI and TREI which represents FOG patterns characterized by small foot speeds. In Fig. 6(a), we model the edges of TREI as spikes and overlay the speed of the foot obtained from the inertial navigation system. In Table II, we list the values assigned to the parameters of the point-process filter. The participant-specific tunable parameter σ_s assigns a unit weight to bin interval with average bin speed zero, as shown in Fig. 6(b). In Fig. 6(c), the region consisting of high density of spikes with small foot speeds corresponds to an increase in the pFOG curve with some delay. We set the pFOG threshold as 0.7. When the pFOG is greater than 0.7, we determine the local minimum of the pFOG curve and denote it as the onset time of FOG. The duration of freezing is determined by subtracting the instant when the pFOG curve goes below 0.7 from the onset time, as indicated with red background in
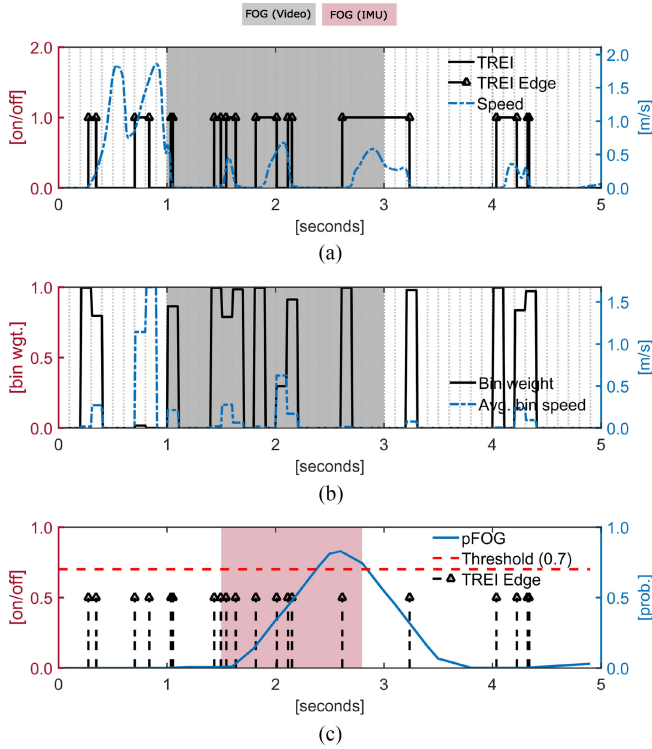
Fig. 6. Detection of FOG using the point-process filter. (a) Spikes with an overlay of foot speed. (b) Bin weights with $\Delta = 0.1$ s and $\sigma_s = 0.4$. (c) pFOG output of the point-process filter.

TABLE II
POINT-PROCESS FILTER PARAMETERS

Parameters of the point-process filter	Assigned value
Width of each bin, Δ	0.1 seconds
Length of each bin, ΔF_s	100 samples
Length of the history of spikes, l	10
Background firing rate, α	-15
Fixed scaling parameter, β	35
State transition matrix, $\boldsymbol{F}_k$	$\boldsymbol{I}_l$
Process noise covariance matrix, $\boldsymbol{Q}_k$	$10^{-14}\boldsymbol{I}_l$
Initial state of the parameter vector, $\boldsymbol{\theta}_{0|0}$	$0.35\mathbb{1}_l$
Initial covariance matrix, $\boldsymbol{P}_{0|0}$	$10^2\boldsymbol{Q}_k$
Participant-specific tunable parameter, σ_s	0.4

Fig. 6(c). Further, on computing the onset and duration of FOG event, we notice a significant overlap between the FOG region detected by processing the IMU data using our proposed system design (represented with red background) and the video data in the reference system (represented with gray background). The mismatch between the FOG region detected using the video and the inertial sensor data in Fig. 6(c) is also attributed to the difference in the temporal resolution of the two systems under consideration.

VIII. EXPERIMENTAL EVALUATION

In this section, we analyze the performance of the system design in Fig. 1, using real data from 16 people with PD. For our sample, there were seven females, the mean age

was 70.3 ± 7.9 years, the mean disease duration was 5.0 ± 3.6 years, and the median off medication Movement Disorders Society Unified Parkinson Disease Rating Scale Motor Subsection (MDS_UPDRS_III) Score was 35.5 (first and third quartiles: 30.5, 41.5). The IMU data and video data for all the participants were recorded for the list of gait tasks in Table I, with the only exceptions being TT006–NARROW and TT006–EIGHT, which were not recorded due to network issues. The true instances of FOG events detected in the video data are manually marked by a trained gait analysis experts. We use the definitions of TPR and FAR in (15) to evaluate the performance of the proposed method for all the tasks listed in Table I. Due to hardware issues with respect to one of the Openshoe modules, data were not available for both feet for all participants. Hence, the data analysis was done using only the left foot inertial sensor data. We also compare our results with an existing method that determines FOG events based on the FI method [19], computed using the vertical axis measurements of the accelerometer data. To calculate the FI [19], we downsample the accelerometer data by a factor of 10 and compute the ratio of the square of the area of the power spectrum in the 'freeze-band' and 'loco-band', using a moving window of 6 seconds. The FI is normalized by multiplying by 100 and taking the natural logarithm.

Out of the sixteen participants, only eight (PID TT003, TT004, TT005, TT007, TT013, TT017, TT021, and TT027) demonstrated FOG. In total, 58 events of FOG were detected using the video data, of which 38 events were categorized as turning freeze, 12 events as initiation or gait freeze, and 8 events as festinating gait with freezing. For each participant, we first identified the task with the greatest number of FOG events to determine the tunable parameters, i.e., the FI-threshold and kernel parameter σ_s. The FI-threshold and kernel parameter were tuned such that the number of FOG events detected was maximized for the identified task. In the proposed method, the system parameters such as detector thresholds, size of the window, standard deviation of the accelerometer and gyroscope, and point-process filter variables remain fixed for all participants across all tasks. Only the participant-specific tunable parameter is adjusted for every participant and remains fixed across all tasks. For participants who demonstrated FOG in the video-based reference system, the individual FI-threshold ranged from 4.5 to 10.0 (mean = 6.56 and s.d. = 1.67), and the kernel parameter σ_s ranged from 0.24 to 0.4 (mean = 0.30 and s.d. = 0.06). We present a detailed analysis of our proposed approach for PID TT027 in Appendix F of the supplementary material. In Tables III and IV, we summarize the number of FOG events detected using FI and our method, respectively. For simplicity, we call our method the pFOG method. Overall, the pFOG method obtained an accuracy of 81.03%, i.e., 47/58 FOG events were detected using a tuned participant-specific kernel parameter (see Table III). Further, when compared with the FI method, our method shows either an improvement or equivalent performance in detecting different types of FOG events (see Table IV). We also compared our proposed approach with the FI method for a fixed value of participant-specific tunable parameter and FI-threshold. These values were obtained by taking the average of these parameters across all FOG participants (see Table III). The results are

TABLE III
NUMBER OF FOG EVENTS DETECTED FOR DIFFERENT PARTICIPANTS ACROSS THE GAIT TASKS

PID	PARAMETER		BACK		BLOCK		EIGHT		NARROW		TURN		TOTAL	
	FI	pFOG	FI	pFOG	FI	pFOG	FI	pFOG	FI	pFOG	FI	pFOG	FI	pFOG
TT003	7.0	0.40	(0/0)	(0/0)	(0/1)	(0/1)	(0/0)	(0/0)	(0/0)	(0/0)	(0/0)	(0/0)	(0/1)	(0/1)
TT004	4.5	0.24	(0/2)	(2/2)	(5/6)	(5/6)	(0/0)	(0/0)	(0/0)	(0/0)	(0/0)	(0/0)	(5/8)	(7/8)
TT005	7.0	0.35	(0/1)	(1/1)	(0/0)	(0/0)	(0/0)	(0/0)	(0/1)	(1/1)	(0/0)	(0/0)	(0/2)	(2/2)
TT007	10.0	0.24	(5/8)	(6/8)	(0/0)	(0/0)	(0/1)	(1/1)	(0/1)	(0/1)	(0/0)	(0/0)	(5/10)	(7/10)
TT013	6.0	0.25	(0/0)	(0/0)	(1/3)	(2/3)	(0/0)	(0/0)	(2/2)	(1/2)	(0/0)	(0/0)	(3/5)	(3/5)
TT017	7.0	0.40	(0/0)	(0/0)	(1/1)	(0/1)	(0/0)	(0/0)	(0/0)	(0/0)	(0/0)	(0/0)	(1/1)	(0/1)
TT021	5.0	0.30	(1/1)	(1/1)	(3/3)	(3/3)	(1/2)	(1/2)	(0/0)	(0/0)	(1/1)	(1/1)	(6/7)	(6/7)
TT027	6.0	0.29	(3/3)	(3/3)	(7/8)	(7/8)	(4/4)	(3/4)	(2/3)	(3/3)	(5/6)	(6/6)	(21/24)	(22/24)
TOTAL	6.56 (avg)	0.30 (avg)	(9/15)	(13/15)	(17/22)	(17/22)	(5/7)	(5/7)	(4/7)	(5/7)	(6/7)	(7/7)	(41/58)	**(47/58)**

TABLE IV
DETECTION PERFORMANCE FOR DIFFERENT TYPES OF FOG EVENTS

Event type (No. of events)	(tuned) FI	(tuned) pFOG
Turn Freeze (38)	71.05% (27)	84.21% (32)
Initiation/Gait Freeze (12)	75.00% (9)	75.00% (9)
Festination with Freeze (8)	62.50% (5)	75.00% (6)
Overall (58)	70.68% (41)	**81.03**% (47)

TABLE V
AVERAGE VALUE OF TPR AND FAR

Performance Metric	FI	pFOG
Avg. FAR (non-FOG participants)	0.07	**0.03**
Avg. TPR (FOG participants)	0.66	0.73
Avg. FAR (FOG participants)	0.21	**0.07**
Avg. TPR (all participants)	0.82	0.86
Avg. FAR (all participants)	0.15	**0.05**

presented in Appendix G of the supplementary material. For a fixed value of the participant-specific tunable parameter, the pFOG method obtained an accuracy of 72.41% whereas the FI method obtained an accuracy of 56.68% (see Table 1 of the supplementary material). This observation motivates the need to develop methods that can automatically adjust the participant-specific tunable parameter based on individual gait patterns.

Next, we compute the TPR and FAR for all participants across all tasks, using video as the reference system. For participants who did not exhibit FOG, the FI-threshold is set to the mean value of the FI-threshold obtained for FOG participants, rounded to the nearest integer. Similarly, for non-FOG participants, the kernel parameter $\sigma_s = 0.4$, a value which assigns a unit weight if the average speed in the bin is zero. We call this the 'baseline setting'. In Table V, we summarize the average values of TPR and FAR for all tasks across all participants. We first notice that the proposed method demonstrates a low average FAR for non-FOG participants using the baseline setting. Next, we observe that the average value of TPR for FOG participants using the proposed and existing method are nearly the same. However, the proposed method demonstrates an overall accuracy of 81.03% (see Tables III and IV). Further, the proposed method shows a more than three-fold decrease in

the average value of FAR for FOG participants. A similar trend is also observed in the average values of TPR and FAR for all tasks across all participants using the pFOG method, displaying an overall improvement in the accuracy of determining the onset and duration of FOG.

IX. SUMMARY AND CONCLUSION

In this paper, we introduced a system design to address the problem of detection of FOG using inertial sensors. We developed a physical model for the sensor data that describes the trembling motion during FOG events. Next, we designed a generalized likelihood ratio test framework to develop a two-stage detector for determining the zero-velocity and trembling events in the gait. We also developed a point-process filter that combines the output of the detectors with information about the speed of the foot, provided by a foot-mounted inertial navigation system, and calculated the probability of FOG. *Our results demonstrate an overall improvement in detecting the number of FOG events and also a three-fold decrease in the false alarm rate when compared with an existing method*. The price paid is an increased computational load and the need for additional sensors (gyroscopes). However, considering that ultra-low-cost IMUs today can be manufactured at cost less than one dollar and that powerful floating point micro-controllers are readily available, advanced signal processing strategies such as that proposed in the paper are practical and feasible for most applications.

In the future, we plan to develop an adaptive design framework which learns the system parameters based on the FOG event and dynamically adjusts the model parameters accordingly. Development of a valid, reliable, and dynamic method of real-time identification of FOG is critical to better understand patterns and frequency of FOG in daily life. An enhanced understanding of FOG may lead to development of novel treatment approaches to address FOG events in real-time.

REFERENCES

[1] H. Braak *et al.*, "Stages in the development of Parkinson's disease-related pathology," *Cell Tissue Res.*, vol. 318, no. 1, pp. 121–134, 2004.

[2] L. M. Shulman *et al.*, "The evolution of disability in Parkinson disease," *Movement Disorders*, vol. 23, no. 6, pp. 790–796, 2008.

[3] N. Giladi and A. Nieuwboer, "Understanding and treating freezing of gait in Parkinsonism, proposed working definition, and setting the stage," *Movement Disorders*, vol. 23, no. S2, pp. S423–S425, 2008.

[4] M. Bachlin *et al.*, "Wearable assistant for Parkinson's disease patients with the freezing of gait symptom," *IEEE Trans. Inf. Technol. Biomed.*, vol. 14, no. 2, pp. 436–446, Mar. 2010.

[5] N. Giladi *et al.*, "Freezing of gait in Parkinson's disease: Prospective assessment in the DATATOP cohort," *Neurology*, vol. 56, no. 12, pp. 1712–1721, 2001.

[6] T. C. Rubinstein *et al.*, "The power of cueing to circumvent dopamine deficits: A review of physical therapy treatment of gait disturbances in Parkinson's disease," *Movement Disorders*, vol. 17, no. 6, pp. 1148–1160, 2002.

[7] A. Nieuwboer, "Cueing for freezing of gait in patients with Parkinson's disease: A rehabilitation perspective," *Movement Disorders*, vol. 23, no. S2, pp. S475–S481, 2008.

[8] G. C. McIntosh *et al.*, "Rhythmic auditory-motor facilitation of gait patterns in patients with Parkinson's disease," *J. Neurol., Neurosurgery Psychiatry*, vol. 62, no. 1, pp. 22–26, 1997. [Online]. Available: http://jnnp.bmj.com/content/62/1/22.abstract

[9] Y. Okuma, "Freezing of gait in Parkinson's disease," *J. Neurol.*, vol. 253, no. 7, pp. VII27–VII32, 2006.

[10] A. Nieuwboer *et al.*, "Reliability of the new freezing of gait questionnaire: Agreement between patients with Parkinson's disease and their carers," *Gait Posture*, vol. 30, no. 4, pp. 459–463, 2009.

[11] H. Mitoma *et al.*, "Characteristics of Parkinsonian and ataxic gaits: A study using surface electromyograms, angular displacements and floor reaction forces," *J. Neurol. Sci.*, vol. 174, no. 1, pp. 22–39, 2000.

[12] A. Nieuwboer *et al.*, "Electromyographic profiles of gait prior to onset of freezing episodes in patients with Parkinson's disease," *Brain*, vol. 127, no. 7, pp. 1650–1660, 2004.

[13] M. Plotnik *et al.*, "Is freezing of gait in Parkinson's disease related to asymmetric motor function?" *Ann. Neurol.*, vol. 57, no. 5, pp. 656–663, 2005.

[14] J. Hausdorff *et al.*, "Impaired regulation of stride variability in Parkinson's disease subjects with freezing of gait," *Exp. Brain Res.*, vol. 149, no. 2, pp. 187–194, 2003.

[15] A. H. Snijders *et al.*, "Gait-related cerebral alterations in patients with Parkinson's disease with freezing of gait," *Brain*, vol. 134, no. 1, pp. 59–72, 2010.

[16] A. Delval *et al.*, "Objective detection of subtle freezing of gait episodes in Parkinson's disease," *Movement Disorders*, vol. 25, no. 11, pp. 1684–1693, 2010.

[17] J. H. Han *et al.*, "Gait analysis for freezing detection in patients with movement disorder using three dimensional acceleration system," in *Proc. 25th Annu. Int. Conf. IEEE Eng. Med. Biol. Soc.*, 2003, vol. 2, pp. 1863–1865.

[18] J. Han *et al.*, "Gait detection from three dimensional acceleration signals of ankles for the patients with Parkinson's disease-related," in *Proc. IEEE Int. Spec. Topic Conf. Inf. Technol. Biomed.*, Ioannina, Greece, 2006, vol. 2628, pp. 1–4.

[19] S. T. Moore *et al.*, "Ambulatory monitoring of freezing of gait in Parkinson's disease," *J. Neurosci. Methods*, vol. 167, no. 2, pp. 340–348, 2008.

[20] E. Jovanov *et al.*, "deFOG—A real time system for detection and unfreezing of gait of Parkinson's patients," in *Proc. Annu. Int. Conf. IEEE Eng. Med. Biol. Soc.*, 2009, pp. 5151–5154.

[21] P. Healthcare, "A wearable system to assist walking of Parkinson's disease patients," *Methods Inf. Med.*, vol. 49, pp. 88–95, 2010.

[22] E. E. Tripoliti *et al.*, "Automatic detection of freezing of gait events in patients with Parkinson's disease," *Comput. Methods Programs Biomed.*, vol. 110, no. 1, pp. 12–26, 2013.

[23] S. Mazilu *et al.*, "GaitAssist: A daily-life support and training system for Parkinson's disease patients with freezing of gait," in *Proc. SIGCHI Conf. Human Factors Comput. Syst.*, 2014, pp. 2531–2540.

[24] S. Mazilu *et al.*, "The role of wrist-mounted inertial sensors in detecting gait freeze episodes in Parkinson's disease," *Pervasive Mobile Comput.*, vol. 33, pp. 1–16, 2016.

[25] M. Bächlin *et al.*, "Wearable assistant for Parkinson's disease patients with the freezing of gait symptom," *IEEE Trans. Inf. Technol. Biomed.*, vol. 14, no. 2, pp. 436–446, Mar. 2010.

[26] K. J. Kubota *et al.*, "Machine learning for large-scale wearable sensor data in Parkinson's disease: Concepts, promises, pitfalls, and futures," *Movement Disorders*, vol. 31, no. 9, pp. 1314–1326, 2016.

[27] A. Nieuwboer *et al.*, "Abnormalities of the spatiotemporal characteristics of gait at the onset of freezing in Parkinson's disease," *Movement Disorders*, vol. 16, no. 6, pp. 1066–1075, 2001.

[28] R. Iansek *et al.*, "The sequence effect and gait festination in parkinson disease: Contributors to freezing of gait?" *Movement Disorders*, vol. 21, no. 9, pp. 1419–1424, 2006. [Online]. Available: http://dx.doi.org/10.1002/mds.20998

[29] S. M. Kay, "Fundamentals of statistical signal processing, vol. II: Detection theory," in *Signal Processing*. Upper Saddle River, NJ, USA: Prentice-Hall, 1998.

[30] B. R. Bloem *et al.*, "Falls and freezing of gait in Parkinson's disease: A review of two interconnected, episodic phenomena," *Movement Disorders*, vol. 19, no. 8, pp. 871–884, 2004.

[31] J. G. Nutt *et al.*, "Freezing of gait: Moving forward on a mysterious clinical phenomenon," *Lancet Neurol.*, vol. 10, no. 8, pp. 734–744, 2011.

[32] M. E. Morris *et al.*, "Stride length regulation in Parkinson's disease normalization strategies and underlying mechanisms," *Brain*, vol. 119, no. 2, pp. 551–568, 1996.

[33] M. Morris *et al.*, "Abnormalities in the stride length-cadence relation in parkinsonian gait," *Movement Disorders*, vol. 13, no. 1, pp. 61–69, 1998.

[34] N. Giladi *et al.*, "Gait festination in Parkinson's disease," *Parkinsonism Related Disorders*, vol. 7, no. 2, pp. 135–138, 2001.

[35] H. M. Schepers *et al.*, "Ambulatory assessment of ankle and foot dynamics," *IEEE Trans. Biomed. Eng.*, vol. 54, no. 5, pp. 895–902, May 2007.

[36] H. M. Schepers *et al.*, "Ambulatory estimation of center of mass displacement during walking," *IEEE Trans. Biomed. Eng.*, vol. 56, no. 4, pp. 1189–1195, Apr. 2009.

[37] A. M. Sabatini *et al.*, "Assessment of walking features from foot inertial sensing," *IEEE Trans. Biomed. Eng.*, vol. 52, no. 3, pp. 486–494, Mar. 2005.

[38] S. J. M. Bamberg *et al.*, "Gait analysis using a shoe-integrated wireless sensor system," *IEEE Trans. Inf. Technol. Biomed*, vol. 12, no. 4, pp. 413–423, Jul. 2008.

[39] J. M. Jasiewicz *et al.*, "Gait event detection using linear accelerometers or angular velocity transducers in able-bodied and spinal-cord injured individuals," *Gait Posture*, vol. 24, no. 4, pp. 502–509, 2006.

[40] E. Foxlin, "Pedestrian tracking with shoe-mounted inertial sensors," *IEEE Comput. Graph. Appl.*, vol. 25, no. 6, pp. 38–46, Nov. 2005.

[41] L. Ojeda and J. Borenstein, "Non-GPS navigation for security personnel and first responders," *J. Navigat.*, vol. 60, no. 3, pp. 391–407, Sep. 2007.

[42] P. Stromback *et al.*, "Foot-mounted inertial navigation and cooperative sensor fusion for indoor positioning," in *Proc. Int. Tech. Meeting Inst. Navigat.*, Jan. 2010, pp. 89–98.

[43] J. O. Nilsson *et al.*, "Foot-mounted inertial navigation made easy," in *Proc. Int. Conf. Indoor Positioning Indoor Navigat.*, Oct. 2014, pp. 24–29.

[44] D. S. Colomar *et al.*, "Smoothing for ZUPT-aided INSs," in *Proc. Int. Conf. Indoor Positioning Indoor Navig.*, Nov. 2012, pp. 1–5.

[45] J. O. Nilsson *et al.*, "Foot-mounted INS for everybody—An open-source embedded implementation," in *Proc. IEEE/ION Position, Location Navigat. Symp.*, Apr. 2012, pp. 140–145.

[46] I. Skog *et al.*, "Zero-velocity detection—An algorithm evaluation," *IEEE Trans. Biomed. Eng.*, vol. 57, no. 11, pp. 2657–2666, Nov. 2010.

[47] J. Farrell, *Aided Navigation: GPS with High Rate Sensors*, 1st ed. New York, NY, USA: McGraw-Hill, 2008.

[48] D. R. Cox and V. Isham, *Point Processes*, vol. 12. Boca Raton, FL, USA: CRC Press, 1980.

[49] A. C. Smith and E. N. Brown, "Estimating a state-space model from point process observations," *Neural Comput.*, vol. 15, no. 5, pp. 965–991, May 2003.

[50] U. T. Eden *et al.*, "Dynamic analysis of neural encoding by point process adaptive filtering," *Neural Comput.*, vol. 16, no. 5, pp. 971–998, May 2004.

[51] A. Ergun *et al.*, "Construction of point process adaptive filter algorithms for neural systems using sequential Monte Carlo methods," *IEEE Trans Biomed. Eng.*, vol. 54, no. 3, pp. 419–428, Mar. 2007.

[52] S. Koyama *et al.*, "Bayesian decoding of neural spike trains," *Ann. Inst. Statist. Math.*, vol. 62, no. 1, pp. 37–59, 2009.

[53] S. Koyama *et al.*, "Approximate methods for state-space models," *J. Amer. Statist. Assoc.*, vol. 105, no. 489, pp. 170–180, 2010.

[54] I. Skog *et al.*, "Evaluation of zero-velocity detectors for foot-mounted inertial navigation systems," in *Proc. Int. Conf. Indoor Positioning Indoor Navigat.*, Sep. 2010, pp. 1–6.